

## Strain-Induced Gauge Field and Landau Levels in Acoustic Structures

Zhaoju Yang,<sup>1</sup> Fei Gao,<sup>1</sup> Yahui Yang,<sup>1</sup> and Baile Zhang<sup>1,2,\*</sup>

<sup>1</sup>*Division of Physics and Applied Physics, School of Physical and Mathematical Sciences, Nanyang Technological University, Singapore 637371, Singapore*

<sup>2</sup>*Centre for Disruptive Photonic Technologies, Nanyang Technological University, Singapore 637371, Singapore*

(Received 26 January 2017; published 12 May 2017)

The emerging field of topological acoustics that explores novel gauge-field-related phenomena for sound has drawn attention in recent years. However, previous approaches constructing a synthetic gauge field for sound predominantly relied on a periodic system, being unable to form a uniform effective magnetic field, thus lacking access to some typical magnetic-induced quantum phenomena such as Landau energy quantization. Here we introduce strain engineering, previously developed in graphene electronics and later transferred to photonics, into a two-dimensional acoustic structure in order to form a uniform effective magnetic field for airborne acoustic wave propagation. Landau levels in the energy spectrum can be formed near the Dirac cone region. We also propose an experimentally feasible scheme to verify the existence of acoustic Landau levels with an acoustic measurement. As a new freedom of constructing a synthetic gauge field for sound, our study offers a path to previously inaccessible magneticlike effects in traditional periodic acoustic structures.

DOI: 10.1103/PhysRevLett.118.194301

Sound waves traveling through air are essentially longitudinal waves, which carry no intrinsic spins and do not respond to magnetic fields. Yet, by constructing gauge fields with different approaches, it is possible to explore magneticlike effects (e.g., the quantum Hall effect [1]) for sound. This is the underlying mechanism supporting the emerging field of topological acoustics [2–12], in which many novel acoustic phenomena have been proposed and achieved in the past few years. However, previous approaches of constructing gauge fields relied on the periodic structures and thus cannot form a uniform effective magnetic field (a uniform magnetic field is associated with a nonperiodic vector potential). As a consequence, some typical magnetic-induced phenomena such as the quantized Landau levels [1] have not been possible for airborne acoustic waves.

It is well known in graphene physics that a strong uniform magnetic field applied on graphene can lead to the quantized electronic conductivity as a result of quantized Landau levels in the energy spectrum [13]. In a magnetic-free circumstance, it has been reported that strained graphene can form a gauge field with an effective magnetic field reaching 300 T [14,15], opening a door to the strain engineering of graphene electronics. Shortly, this idea of strain engineering has been introduced into photonics [16], where a strained honeycomb photonic lattice, being invariant along the  $z$  direction, can form photonic Landau levels. However, these photonic Landau levels refer to the quantization of  $k_z$  momentum, rather than the energy (frequency), being fundamentally difficult to be implemented in a two-dimensional (2D) geometry.

Here we introduce the strain-induced gauge fields into a 2D acoustic structure hosting airborne (longitudinal) acoustic waves. The strain effect makes the acoustic lattice

aperiodic, which can be realized by simply displacing the lattice sites away from their original positions. The strain-induced gauge field corresponds to a strong uniform magnetic field, enabling the emergence of discretized Landau levels separated by significant band gaps. Comparing the previously demonstrated photonic Landau levels [16] and the acoustic Landau levels studied in the current work, one can find the following fundamental distinctions. First, the photonic Landau levels are discrete momentum levels of wave number  $k_z$ , while the current acoustic Landau levels are energy levels. Second, the previous photonic Landau levels are demonstrated in a three-dimensional structure whose  $z$  dimension should be infinitely long, while the current acoustic Landau levels are designed in a 2D geometry.

We start with an acoustic honeycomb lattice. The unit cell of the lattice consists of two identical acoustic resonators (cylinders  $A$  and  $B$ ) connected with a thin cylindrical coupling waveguide, as shown in Fig. 1(a). Their geometrical parameters will be given later. The system is filled with air, and the blue surfaces in Fig. 1(a) are treated as acoustic hard boundaries. The lattice constant and nearest-neighbor distance between two sites are  $a_0 = \sqrt{3}a$  and  $a$ , respectively. This lattice of acoustic resonators can be described by the coupled-mode equation [6,8,16]  $i\partial_t p_n = \sum_{\langle m \rangle} \kappa(|\mathbf{r}_{n,m}|) p_m$ , where  $p_n$  is the amplitude of the mode for the  $n$ th resonator,  $\kappa$  is the coupling strength between two resonators, and the summation is taken over the nearest-neighbor resonators. The coupling strength  $\kappa$ , which is physically realized by the coupling waveguide, decays almost exponentially as the nearest-neighbor distance increases [17]. Here we assume that the coupling strength takes the form of function  $\kappa = \kappa_0 \exp[-\beta(r/a - 1)]$  as it is

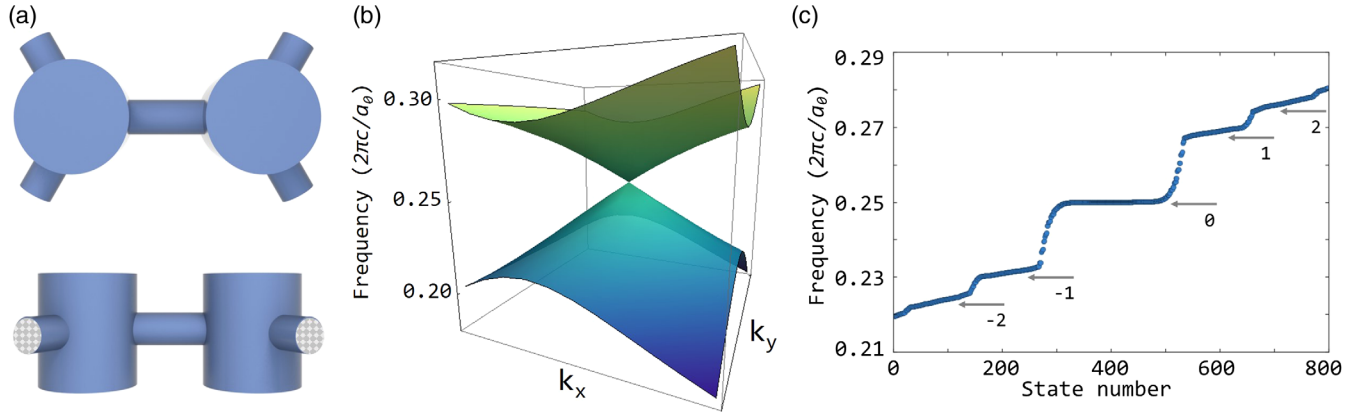


FIG. 1. (a) Top and side views of a unit cell of the acoustic honeycomb lattice. The unit cell consists of two identical resonators at inequivalent sites. Each pair of nearest-neighbor resonators is connected with a thin coupling waveguide. (b) The Dirac cone spectrum in a square area with a side length of  $0.4\pi/a$  located at a corner of the Brillouin zone. (c) Triaxial-strain-induced acoustic Landau levels near the Dirac region. A disk with radius  $40a_0$  which consists of 11 600 resonators is adopted in the calculation. The strength of the triaxial strain is  $q = 0.004/a$ . The numbers indicate the orders of Landau levels.

in graphene [13,18], where  $\kappa_0$  is the coupling strength for  $r = a$  and  $\beta$  describes the decay rate of the coupling strength (both values can be retrieved from data fitting). By considering only the lowest two acoustic eigenmodes, the solution to the coupled-mode equation can be equivalent to the one to the tight-binding Hamiltonian of graphene. As a result, at each of the six corners of the Brillouin zone, the energy bands will be expected to cross at the Dirac point. In the following, we choose the radius and height of each resonator as  $r = 0.3a$  and  $h = 2a/3$ , respectively. The coupling waveguide connecting resonators  $A$  and  $B$  has the radius of  $r_c = 0.1a$ . We numerically calculate the band structure of the acoustic honeycomb lattice with a finite-element method, in a square area (side length  $0.4\pi/a$ ) centered at a corner of the first Brillouin zone, as shown in Fig. 1(b). It can be seen that the lowest two bands exhibit the Dirac cone spectrum in the valley  $K$  [near  $\pi/a_0(4/3, 0)$ ]. The frequency at the Dirac point is  $0.255 \times 2\pi c/a_0$  (or 5041 Hz for  $a = 0.01$  m), where  $c$  is the speed of sound in air.

It has been reported that a 2D strain field can induce a gauge field with the vector potential  $A(r) = (\beta/a_0)(u_{xx} - u_{yy}, -2u_{xy})$ , where  $u_{xx}$ ,  $u_{yy}$ , and  $u_{xy}$  are the elements of the strain tensor [14]. The sign of the vector potential for a valley can be changed by switching to another valley. The magnetic field then can be calculated as  $B(r) = \nabla \times A$  (given units  $\hbar/e = 1$ ). By designing a particular form of the strain tensor, a vector potential corresponding to a uniform magnetic field can be achieved. It has been found in both a graphene lattice [14] and a photonic honeycomb lattice [16] that a triaxial strain can fulfill this requirement. In the following, we apply the triaxial strain on the acoustic honeycomb lattice by simply displacing the lattice sites away from their original positions and connecting nearest-neighbor resonators with coupling waveguides of the proper length. The space-dependent displacement for each resonator is given by  $(d_x, d_y) = q(2xy, x^2 - y^2)$ , where  $x$  and  $y$  are the original

location of the resonator and  $q$  describes the strength of the strain. This displacement will construct the vector potential  $A(r) = (4\beta q/a_0)(y, -x)$ , which leads to a uniform magnetic field  $B = 8\beta q/a_0$ .

Once the pseudomagnetic field is formed, Landau levels can emerge in the energy spectrum. To demonstrate the existence of acoustic Landau levels, we first calculate the eigenvalues of a large lattice in the tight-binding limit. We adopt a honeycomb disk with radius  $40a_0$ , which contains 11 600 resonators. A triaxial strain with strength  $q = 0.004/a$  is applied. The parameters of  $\kappa_0 = 0.056 \times c/a_0$  and  $\beta = 1.271$  are retrieved by fitting the data from a finite-element simulation [17]. Figure 1(c) shows, in ascending order of the state number, the calculated 800 eigenvalues near the Dirac cone region for the strained lattice. It can be clearly seen that highly degenerate states and flat levels emerge in the energy spectrum. As a result, the acoustic quasiparticle subjected to this effective magnetic field can follow only cyclotron orbits with discrete energy values. The energy gaps of Landau levels are proportional to  $\sqrt{BN}$  ( $N$  is the level number), being consistent with the behavior of Dirac fermions in a strong magnetic field. Note that the states connecting the discretized Landau levels are localized on the edges. It is these edge states that contribute to the Hall conductivity in the quantum Hall effect [1,13].

To facilitate potential experiments, we now consider a smaller disk with radius  $6a_0$ , which contains only 262 resonators. The triaxial strain with different strengths of  $q = 0.000/a$ ,  $q = 0.015/a$ , and  $q = 0.030/a$  are applied to the disks, as shown in Figs. 2(a)–2(c), respectively. Note that the strain strength  $q = 0.030/a$ , if a piece of graphene were strained to this extent, would yield a pseudomagnetic field of 8590 T. The eigenvalues of the states calculated from commercial software COMSOL Multiphysics are shown in Figs. 2(d)–2(f) for the three cases ordered with increasing

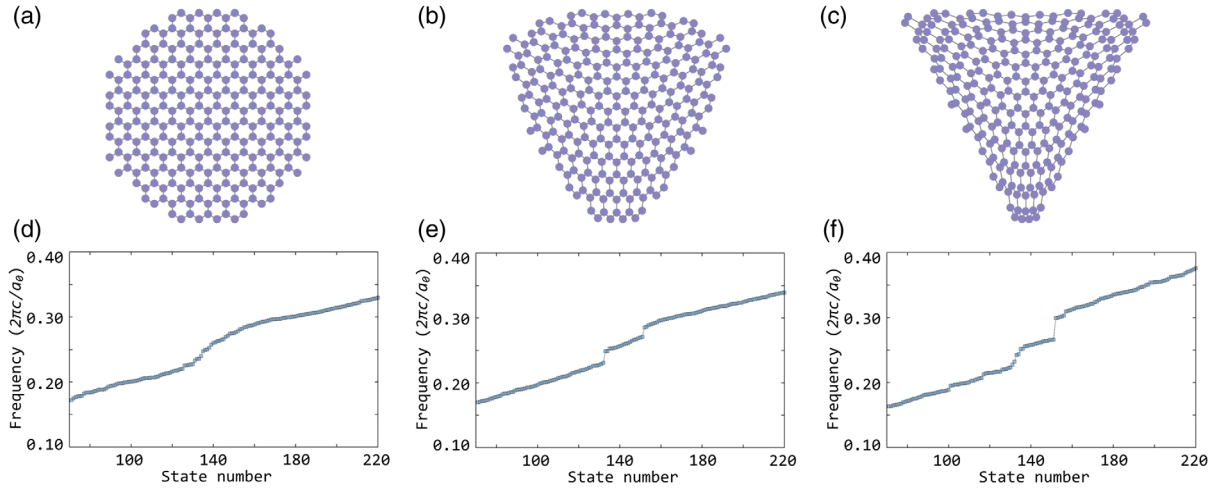


FIG. 2. (a)–(c) Schematics of the unstrained and strained acoustic lattices with increasing strength of triaxial strain (a)  $q = 0.000/a$ , (b)  $q = 0.015/a$ , and (c)  $q = 0.030/a$ . A disk is adopted in the calculation. It has a radius of  $6a_0$  which consists of 262 resonators. (d)–(f) The eigenvalues of the acoustic lattices are plotted in terms of the state number in the ascending order. (d) Without strain, the frequency spectrum shows a continuous behavior. (e),(f) The band gaps emerge and widen with increasing strain.

strain. In Fig. 2(d), the unstrained lattice shows a continuous eigenfrequency spectrum near the Dirac cone region, whereas for the triaxially strained lattice in Fig. 2(e) with strain strength  $q = 0.015/a$ , the Landau energy quantization emerges and results in band gaps between the 0th-order and  $\pm 1$ st-order Landau levels in the frequency ranges of

$(0.231, 0.252) \times 2\pi c/a_0$  and  $(0.267, 0.286) \times 2\pi c/a_0$ . With the increased strain of  $q = 0.030/a$  in Fig. 2(f), as the effective magnetic field doubles, these band gaps expand to frequency ranges of  $(0.223, 0.252) \times 2\pi c/a_0$  and  $(0.266, 0.298) \times 2\pi c/a_0$ . In other words, the gap sizes in Fig. 2(f) are roughly 1.5 times those in Fig. 2(e), being

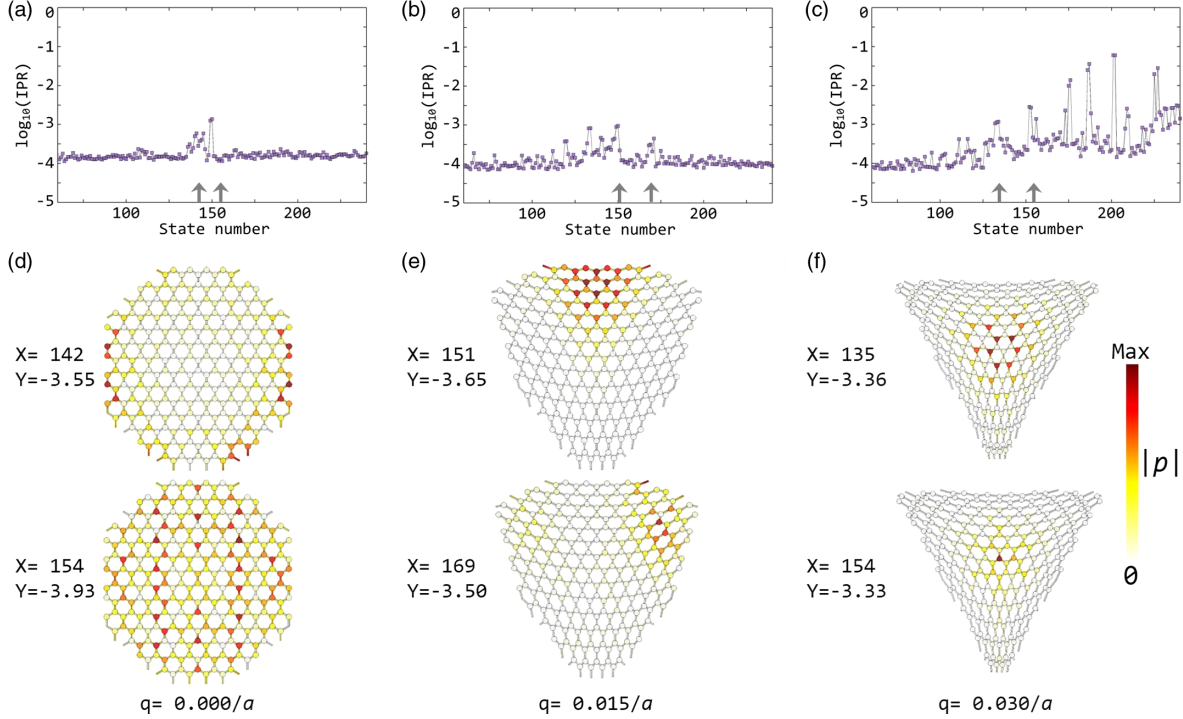


FIG. 3. The logarithmic plots of inverse participation ratio values for the strain strength of (a)  $q = 0.000/a$ , (b)  $q = 0.015/a$ , and (c)  $q = 0.030/a$ , respectively. With increasing IPR values, the eigenstates become more and more localized. (d)–(f) The localization features of the eigenstates with different IPR values for the lattice with a strength of strain (d)  $q = 0.000/a$ , (e)  $q = 0.015/a$ , and (f)  $q = 0.030/a$ .  $X$  represents the state number, and  $Y$  is  $\log_{10}(\text{IPR})$ . The thermal color indicates the amplitude of the acoustic pressure.

consistent with the energy gaps of Landau levels that increase as  $\sim\sqrt{BN}$ . With increased strain, the states of the 0th-order Landau level becomes more flat and thus achieves higher degeneracies, leading to slower acoustic wave propagation. There can be relatively more edge states connecting the Landau levels, as is seen in Fig. 2(f) between the  $-1$ st-order and 0th-order levels. Note that the Landau levels of higher orders can also be labeled, in principle, based on the relationship of  $\sim\sqrt{BN}$ , where the coefficient can be obtained through data fitting.

The localization feature of the eigenstates can be characterized by calculating the inverse participation ratio [19,20], i.e.,  $\text{IPR} = \int |p|^4 dr / (\int |p|^2 dr)^2$ , where  $p$  is the acoustic pressure. The IPR value is a measure of the portion of the space where the amplitude of the wave function differs markedly from zero. A small value of the IPR corresponds to a delocalized (extended) state, whereas a large value means the state is localized. Figures 3(a)–3(c) show the logarithmic plots of the IPR for the above three strain strengths. For the unstrained lattice, most  $\log_{10}(\text{IPR})$  values are maintained around  $-3.9$ . These states are all extended states, one of which is demonstrated in the lower panel in Fig. 3(d), where the color represents the amplitude

of the acoustic pressure. Several states near the state number 142 (near the Dirac point) acquire relatively high  $\log_{10}(\text{IPR})$  values because of their localization at the edges. One example with a  $\log_{10}(\text{IPR})$  value of  $-3.55$  is shown in the upper panel in Fig. 3(d). When the strain increases, the values of  $\log_{10}(\text{IPR})$  near the Dirac region (state number ranges from about 100 to 200) increase, indicating that states become more and more localized. Note that the sharp peaks with  $\log_{10}(\text{IPR})$  values around  $-2$  in Fig. 3(c) are the strongly confined edge states localized in the coupling waveguides at edges. To demonstrate the localized states in detail, we plot the eigenstate pattern in Figs. 3(d)–3(f). For the strain with a strength of  $q = 0.015/a$ , the states with numbers of 151 and 169 [ $\log_{10}(\text{IPR})$  values of  $-3.65$  and  $-3.50$ , respectively] are shown in Fig. 3(e). For the strain with a strength of  $q = 0.030/a$ , the states with numbers of 135 and 154 [ $\log_{10}(\text{IPR})$  values of  $-3.36$  and  $-3.33$ , respectively] are demonstrated in Fig. 3(f). The acoustic pressure patterns manifest that the strain introduces localized states not only on the edges but also inside the bulk of the sample.

We then propose a simple scheme that can be adopted in an experiment to verify the existence of Landau levels

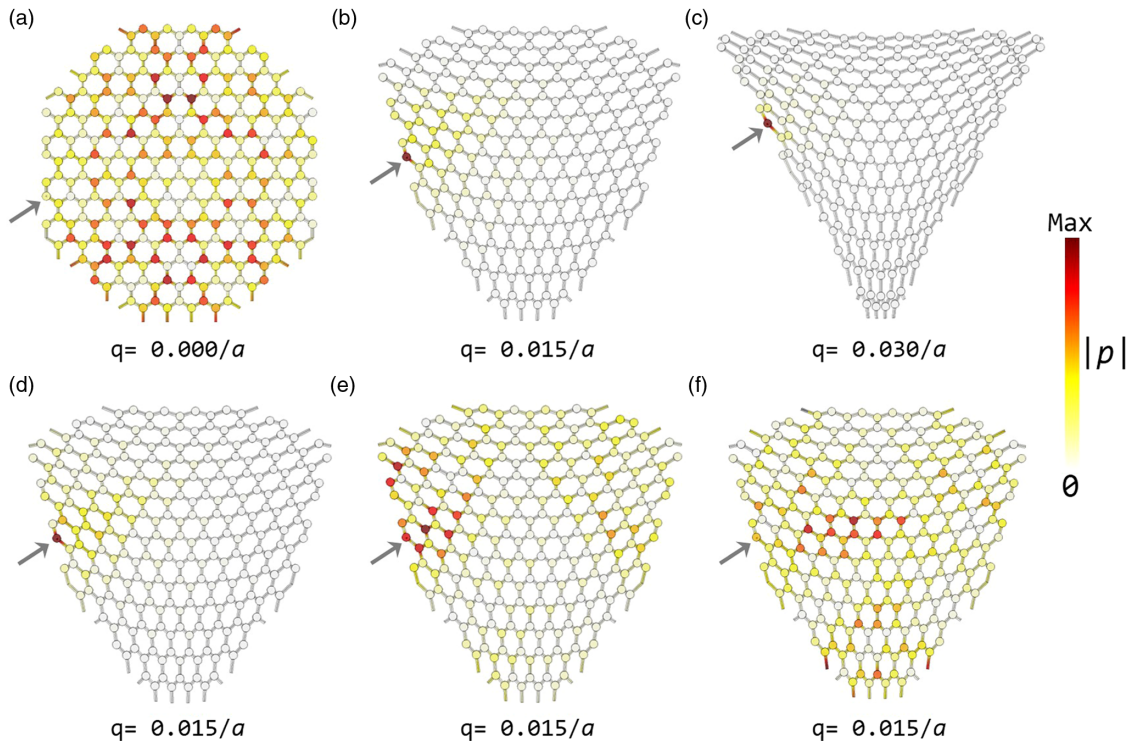


FIG. 4. (a)–(c) The excitation of acoustic waves at the edges of the unstrained and strained lattices with the strength of (a)  $q = 0.000/a$ , (b)  $q = 0.015/a$ , and (c)  $q = 0.030/a$ . The operating frequency of the source is  $0.281 \times 2\pi c/a_0$  (5565 Hz). The black arrow points to the location of the acoustic source. The extended state is excited in panel (a). Highly confined states are excited in panels (b) and (c), because the frequency locates in the band gap between 0th-order and 1st-order Landau levels. (d)–(f) In the aperiodic lattice with a strain strength of  $q = 0.015/a$ , the excitation frequency of the source is (d)  $0.237 \times (2\pi c/a_0)$ , (e)  $0.261 \times (2\pi c/a_0)$ , and (f)  $0.293 \times (2\pi c/a_0)$ , respectively. The intensity profiles show the transition from localization (d) to spreading (e) to localization (b) to spreading (f). The thermal color indicates the amplitude of the acoustic pressure.

with an acoustic measurement. By fixing the operating frequency of  $0.281 \times 2\pi c/a_0$  (or 5565 Hz for  $a = 0.01$  m), we can put a sound source, as indicated by the black arrow in Figs. 4(a)–4(c), at edges of the unstrained and strained lattices, to excite the same resonator. In Fig. 4(a), the acoustic pressure spreads into the bulk of the unstrained lattice because of the excitation of the extended bulk state. For strained lattices, the Landau levels emerge, and the current operating frequency locates inside the band gap between the 0th-order and 1st-order Landau levels. As a result, in Fig. 4(b), the strong localization on one edge makes the sound energy confined. The larger band gap in Fig. 4(c) leads to a shorter decay length and tighter confinement. To further verify the Landau quantization in the frequency spectrum, we choose the strained lattice in Fig. 4(b) and simulate the acoustic field by setting the source frequency to  $0.237 \times 2\pi c/a_0$ ,  $0.261 \times 2\pi c/a_0$ , and  $0.293 \times 2\pi c/a_0$  (or 4700, 5158, and 5808 Hz for  $a = 0.01$  m) as shown in Figs. 4(d)–4(f), respectively. Figure 4(d) shows that the acoustic pressure profile is confined at the edge, because the frequency locates in the band gap between  $-1$ st-order and 0th-order Landau levels. The acoustic wave that spreads into the bulk in Fig. 4(e) demonstrates one localized eigenstate within the 0th-order Landau level. With a higher frequency as in Fig. 4(f), the acoustic wave again spreads into the bulk. Together with the acoustic pressure profile in Fig. 4(b), this process of localization-spreading-localization-spreading as the frequency increases can verify the existence of Landau levels as well as the band gaps between them.

In conclusion, we introduce the strain-induced gauge fields into an acoustic structure and construct a uniform effective magnetic field that is difficult in previous periodic acoustic structures. This uniform magnetic field enables the emergence of discretized Landau levels separated by significant band gaps in the energy spectrum for airborne acoustic wave propagation. The strong gauge field generated in acoustics and the simple implementation approach open the door to previously inaccessible magneticlike effects, which may find use in sound enhancement as in nonlinear acoustics and sound sensing as in biomedical imaging.

This work was sponsored by Nanyang Technological University under NAP Start-Up Grants and Singapore Ministry of Education under Grants No. Tier 1 RG174/16(S), No. MOE2015-T2-1-070 and No. MOE2011-T3-1-005.

*Note added.*—Recently, we came across a preprint [21] proposing an application of strain engineering in mechanical metamaterials to engineer Landau levels for lattice vibrations.

\*To whom correspondence should be addressed.

blzhang@ntu.edu.sg

- [1] K. von Klitzing, *Rev. Mod. Phys.* **58**, 519 (1986).
- [2] R. Fleury, D. L. Sounas, C. F. Sieck, M. R. Haberman, and A. Alu, *Science* **343**, 516 (2014).
- [3] Z. Yang, F. Gao, X. Shi, X. Lin, Z. Gao, Y. Chong, and B. Zhang, *Phys. Rev. Lett.* **114**, 114301 (2015).
- [4] N. Xu, H. Cheng, S. Xiao-Chen, L. Xiao-ping, L. Ming-Hui, F. Liang, and C. Yan-Feng, *New J. Phys.* **17**, 053016 (2015).
- [5] A. B. Khanikaev, R. Fleury, S. H. Mousavi, and A. Alù, *Nat. Commun.* **6**, 8260 (2015).
- [6] M. Xiao, W.-J. Chen, W.-Y. He, and C. T. Chan, *Nat. Phys.* **11**, 920 (2015).
- [7] M. Xiao, G. Ma, Z. Yang, P. Sheng, Z. Q. Zhang, and C. T. Chan, *Nat. Phys.* **11**, 240 (2015).
- [8] Z. Yang and B. Zhang, *Phys. Rev. Lett.* **117**, 224301 (2016).
- [9] C. He, X. Ni, H. Ge, X.-C. Sun, Y.-B. Chen, M.-H. Lu, X.-P. Liu, and Y.-F. Chen, *Nat. Phys.* **12**, 1124 (2016).
- [10] J. Lu, C. Qiu, L. Ye, X. Fan, M. Ke, F. Zhang, and Z. Liu, *Nat. Phys.* (to be published).
- [11] Y. G. Peng, C. Z. Qin, D. G. Zhao, Y. X. Shen, X. Y. Xu, M. Bao, H. Jia, and X. F. Zhu, *Nat. Commun.* **7**, 13368 (2016).
- [12] Z. Yang, F. Gao, X. Shi, and B. Zhang, *New J. Phys.* **18**, 125003 (2016).
- [13] A. H. Castro Neto, F. Guinea, N. M. R. Peres, K. S. Novoselov, and A. K. Geim, *Rev. Mod. Phys.* **81**, 109 (2009).
- [14] F. Guinea, M. I. Katsnelson, and A. K. Geim, *Nat. Phys.* **6**, 30 (2010).
- [15] N. Levy, S. A. Burke, K. L. Meaker, M. Panlasigui, A. Zettl, F. Guinea, A. H. C. Neto, and M. F. Crommie, *Science* **329**, 544 (2010).
- [16] M. C. Rechtsman, J. M. Zeuner, A. Tunnermann, S. Nolte, M. Segev, and A. Szameit, *Nat. Photonics* **7**, 153 (2013).
- [17] See Supplemental Material at <http://link.aps.org/supplemental/10.1103/PhysRevLett.118.194301> for details of Retrieving the parameters of  $\kappa_0$  and  $\beta$ .
- [18] V. M. Pereira, A. H. Castro Neto, and N. M. R. Peres, *Phys. Rev. B* **80**, 045401 (2009).
- [19] B. Kramer and A. MacKinnon, *Rep. Prog. Phys.* **56**, 1469 (1993).
- [20] M. P. Marder, *Condensed Matter Physics* (Wiley, New York, 2010).
- [21] H. Abbaszadeh, A. Souslov, J. Paulose, H. Schomerus, and V. Vitelli, [arXiv:1610.06406](https://arxiv.org/abs/1610.06406).